

Robust projected weakening of winter monsoon winds over the Arabian Sea under climate change

V. Parvathi¹, I. Suresh¹, M. Lengaigne^{2,3}, T. Izumo^{2,3}, J. Vialard²

¹ CSIR-National Institute of Oceanography (CSIR-NIO), Goa, India

² Sorbonne Universités (UPMC, Univ Paris 06)-CNRS-IRD-MNHN, LOCEAN Laboratory, IPSL, Paris, France

³ Indo-French Cell for Water Sciences, IISc-NIO-IITM-IRD Joint International Laboratory, NIO, Goa, India

Submitted to GRL

Corresponding author: I. Suresh
Physical Oceanography Division
National Institute Of Oceanography
Dona Paula – 403004,
Goa, India
Email: isuresh@nio.org

Abstract: The response of the Indian winter monsoon to climate change has received considerably less attention than that of the summer monsoon. We show here that all Coupled Model Intercomparison Project phase-5 (CMIP5) models display a consistent reduction (of 6.5% for Representative Concentration Pathways 8.5 and 3.5% for 4.5, on an average) of the winter monsoon winds over the Arabian Sea at the end of 21st century. This projected reduction weakens, but remains robust when corrected for overestimated Arabian Sea winds in CMIP5. This weakening is driven by reduction in the interhemispheric sea level pressure gradient resulting from enhanced warming of the dry Arabian Peninsula relative to the southern Indian Ocean. The wind weakening reduces winter oceanic heat losses to the atmosphere and deepening of convective mixed layer in the northern Arabian Sea, and hence can potentially inhibit the seasonal chlorophyll bloom that contributes substantially to the Arabian Sea annual productivity.

1. Introduction

The Indian subcontinent experiences the most energetic and vigorous monsoon system globally [Webster *et al.*, 1998; Gadgil, 2003]. During boreal summer, the Asian continent warms faster than the Indian Ocean (IO), favoring the northward movement of the Inter-Tropical Convergence Zone [Trenberth *et al.* 2000] and the development of a low-level cross-equatorial jet [Findlater, 1971; Fig. S1a]. The associated southwesterly winds transport moisture collected over the southern IO and the Arabian Sea (AS) towards the Indian subcontinent, giving rise to the Indian Summer Monsoon (ISM) rainfall. As the livelihood of this densely populated region critically depends on this water supply [Gadgil and Gadgil, 2006], a large body of literature has already investigated the influence of anthropogenic climate change on the ISM [e.g. Goswami *et al.*, 2006; Turner and Annamalai, 2012; Roxy *et al.*, 2015]. Comparisons of present and future simulations from the Coupled Model Intercomparison Project Phase-5 (CMIP5) indicate a consistent increase of future ISM rainfall [e.g. Ogata *et al.*, 2014; Sooraj *et al.*, 2015; Sharmila *et al.*, 2015; Endo and Kitoh, 2016], as well as a general weakening of the large-scale ISM circulation [Sooraj *et al.*, 2015] and poleward shift of the AS low-level jet [Sandeep and Ajayamohan, 2015; Figs. S1b,c,d].

During boreal winter, the Eurasian continent cools while the southern tropical IO warms. The resulting high pressure over the Arabian Peninsula and low pressure under the ITCZ around 10°S drive the Indian Winter Monsoon (IWM), characterized by northeasterly winds over the AS (Fig. 1a). While IWM contributes significantly to the annual precipitation over the Himalayan region [e.g. Dimri *et al.*, 2015] and the southeastern India and Sri Lanka [e.g. Rajeevan *et al.*, 2012; Vialard *et al.*, 2011], most of the rainfall occurs over the ocean around 10°S, thereby forming only a small fraction of the annual rainfall over India. Nonetheless the winter monsoon has its most important implications for the biogeochemistry and ecosystems of the northern IO [e.g. Smith and Madhupratap, 2005]. The evaporative cooling associated with the cold and dry IWM winds induces convective overturning in the northern AS, contributing to the ventilation of the nearly anoxic subsurface waters [Morrison *et al.*, 1999]. The convective overturning also entrains nutrients into the surface euphotic layer [Prasanna *et al.*, 2001; Keerthi *et al.*, 2016], leading to a prominent chlorophyll bloom [e.g. Banse and McClain, 1986]. This bloom contributes substantially to the total annual AS primary productivity [Madhupratap *et al.*, 1996; Marra and Barber, 2005] and occurs when the winter oceanic conditions are more favorable for fishing activities than the summer leading to highest fish catch [Madhupratap *et al.*, 2001].

There is to date no study focusing on the projected IWM response to the global warming. Given its importance for the AS climate and biogeochemistry, the present study aims at assessing the

influence of global warming on the IWM by analyzing the present-day and the future simulations from CMIP5 models. This paper is organized as follows. Section 2 introduces the data and methods. Section 3 shows that there is a weakening of IWM winds over the Arabian Sea in CMIP5 models, under both RCP8.5 and 4.5 scenarios, even when model bias is accounted for. Furthermore, this section discusses the impacts and the possible underlying mechanisms of this monsoon weakening. Finally, Section 4 summarizes the results, and discusses their limitations and implications.

2. Data and Methodology

2.1 Data

In this study, we compare the historical simulations (HIST) forced by the observed anthropogenic and natural forcing with the future simulations performed under two contrasted Representative Concentration Pathways (RCP) scenarios: RCP8.5, an unmitigated scenario with radiative forcing reaching 8.5 W.m^{-2} by 2100, and RCP4.5, a mitigated scenario with radiative forcing reaching 4.5 W.m^{-2} by 2100 [Moss *et al.*, 2010]. We analyze monthly mean outputs from 27 CMIP5 models for which 10-m surface winds are available for historical, RCP8.5 and RCP4.5 simulations. When several ensemble members are available, we choose only the first one, in order to assign the same weight to all models. When available, we analyze the monthly precipitation, surface skin temperature (Tsurf), mean sea level pressure (SLP), wind stress, net surface heat flux (HFlx) and mixed layer depth (MLD) from these models. Details on the available variables for each model are provided in Table ST1.

The biases in historical simulations are computed over the 1986-2005 period relative to Tropflux [Praveen Kumaret *al.*, 2012] for surface winds at 10 m, surface temperature and air-sea fluxes; ERA-Interim [Dee *et al.*, 2011] for SLP; and *de Boyer Montegut et al.* [2004] climatology for MLD.

2.2 Methodology

The seasonal average for winter monsoon is defined as the December-March (DJFM) average and that for summer monsoon as the June-September (JJAS) average. In order to allow a fair comparison, all datasets are re-gridded to a common $1^\circ \times 1^\circ$ horizontal grid. We define the present-day climatology of individual models as the 20-year (1986–2005) mean of historical simulations, the future climate as the 20-year (2080–2099) mean of RCP8.5 and RCP4.5 simulations, and the projected climate change as their difference (i.e. RCP minus HIST). We show the Multi Model Mean (MMM) of either the projected response to climate change or bias in order to highlight the consensus across models. As in previous studies [e.g. Christensen *et al.*, 2013], medium (high) robustness is

defined when at least 70% (90%) of models agree on the sign of the projected change or bias.

3. Results

3.1 Robust weakening of the winter monsoon circulation

Figure 1b illustrates that the projected RCP8.5 MMM winter surface winds weaken over most of the IO, except in the Bay of Bengal. This widespread weakening is robust in more than 70% of models over most of the IO (black circles on Fig. 1b), with largest and most coherent changes over the AS and western equatorial IO, where more than 90% of the models agree (red dots on Fig. 1b). Red bars on Figure 1c further detail the percentage of AS average wind speed reduction relative to the present climate average for each model in the RCP8.5 scenario. Every model (out of the 27 for which surface winds are available) projects a weakening of winter winds over the AS by the end of the 21st century, ranging from 2 to 13%. The projected RCP8.5 MMM AS wind reduction is $6.4 \pm 0.9\%$, at the 95% confidence level. Blue bars on Figure 1c illustrate that this wind reduction, although weaker, is also very robust when considering the more optimistic RCP4.5 scenario. In this case, the AS wind reduction ranges from 2 to 6%, with MMM reduction of $3.6 \pm 0.5\%$ at 95% level.

This consistent weakening of the IWM circulation in future CMIP5 simulations may however result as an artifact of the present-day model biases in the IO. *Li et al.* [2016a] for instance showed that most CMIP5 models overestimate the present-day amplitude of the IO dipole (IOD), the main intrinsic mode of interannual SST variations in the IO [e.g. *Saji et al.* 1999]. They further suggest that this overestimation largely explains the consistent IOD-like warming response to climate change in most CMIP5 models, with a stronger IOD-like warming pattern in models with higher IOD amplitude. There is however no relation between the projected AS wind weakening and the IOD amplitude in CMIP5 models ($r=0.15$, not significant at the 90% level; not shown). On the other hand, CMIP models display other biases, which may influence the projected IWM response to climate change. For instance, most CMIP models tend to display a strong IWM, leading to a cold SST bias over the AS [*Sperber et al.*, 2013], which has received some attention because it leads to unrealistic rainfall in the following summer monsoon by reducing the evaporation over the AS [*Levine et al.*, 2013; *Marathayil et al.*, 2013; *Sandeep and Ajayamohan*, 2014].

Figure 2a illustrates this strong IWM winds bias in the CMIP5 MMM, with an overestimated cross-equatorial jet over the western IO and IWM circulation over the AS. The present-day AS wind speeds are on an average overestimated by $\sim 0.6 \text{ m.s}^{-1}$ ($\sim 9\%$). The amplitude and sign of this bias however varies considerably amongst models (Fig. 2b), ranging from a weak underestimation of -0.4 m.s^{-1} to a strong overestimation of 1.5 m.s^{-1} . The amplitude of the AS winter wind reduction in the

RCP8.5 scenario is related to the amplitude of the IWM wind bias ($r=-0.57$ significant at 99% level): models with larger IWM climatological winds (and thus larger bias) generally predict a larger reduction of IWM circulation (Fig. 2b). We can hence adopt a strategy similar to that of *Li et al.* [2016a] and use the statistical linear relation between the model bias and the projected response to climate change to extrapolate the response to that at zero bias (computational details provided in the online Supporting Information). This statistical strategy, known as “emergent constraints”, has already been widely used to provide reliable future projections [e.g., *Bracegirdle and Stephenson*, 2012, 2013; *Cox et al.*, 2013; *Li et al.*, 2016b].

The resulting corrected RCP8.5 surface wind changes are displayed on Figure 2c. The RCP8.5 MMM winter winds over the AS exhibit weakening even when accounting for the present-day IWM biases. The amplitudes of the uncorrected and corrected RCP8.5 projected AS wind speed changes are provided on Figure 2d. Although reduced when applying the bias correction, there is still a robust IWM circulation reduction in response to climate change in all models (Fig. 2d, MMM AS wind reduction with correction is $4.5\pm 0.9\%$ at the 95% confidence level against $6.4\pm 0.9\%$ without correction). The projected weakening is also robust when applying the bias correction to RCP4.5 projections ($2.5\pm 0.5\%$, Fig. S2). Thus the projected IWM circulation weakening is robust in all of the analyzed CMIP5 models under different scenarios, even after accounting for the present-day model biases. Henceforth, for conciseness, we discuss only the RCP8.5 projections, though our conclusions hold true for RCP4.5 projections as well.

3.2 Impacts of the projected IWM weakening

As mentioned in the introduction, the RCP8.5 projected summer monsoon response is associated with a consistent $20\pm 6\%$ increase in rainfall over India (Figs. S3a,c) [*Ogata et al.*, 2014; *Sooraj et al.*, 2015; *Sharmila et al.*, 2015; *Endo and Kitoh*, 2016]. The climate change also induces increased rainfall in the winter monsoon rainy zones in the equatorial IO (Figs. S3b,d). This projected rainfall increase is however weaker ($\sim 10\pm 2\%$; Fig. S3d vs. S3c) and occurs mostly over the ocean, and hence is of lesser relevance from a socio-economic viewpoint compared to its summer counterpart, except for the east African countries and islands located in the equatorial region.

On the other hand, the IWM has important implications for the AS biogeochemistry. The cold and dry air blowing from the continent induces strong evaporative heat losses to the atmosphere in the northern AS. This combines with the mechanical stirring by the northeasterly winds to induce a mixed layer deepening, which in turn drives the winter blooms in the northern AS [*Banse and McClain*, 1986; *Morrison et al.*, 1999; *Madhupratap et al.*, 1996]. Figure 3 shows the projected IWM

surface HFlx and MLD responses. The surface wind weakening induces a reduction of the latent cooling, which is strongest in the northern AS, where the thermo-dynamical imbalance between the ocean and cold, dry IWM winds is largest (Fig. 3a). All but three models exhibit a reduction of the winter surface heat losses in the northern AS (Fig. 3c, $15\pm 5\%$ at 95% confidence level for RCP8.5 MMM; $10\pm 5\%$ when corrected for the wind bias). The surface cooling reduction is strongly correlated ($r=-0.78$, 99% level confidence; Fig. S4a) with the wind reduction over the northern AS, suggesting that the wind weakening drives latent and thus net heat flux reduction.

Air-sea fluxes of momentum have a quadratic dependence on the winds, and hence would reduce roughly twice as that of the wind reduction in terms of the percentage. Indeed, the projected AS wind weakening also reduces the momentum flux at the air-sea interface, leading to a consistent wind stress reduction over the AS (Fig. S5), which is more than two times the wind reduction in percentage ($-15\pm 2\%$ at 95% confidence level for RCP8.5 MMM; Fig. S5c). The reduced heat losses at the surface and the reduced mechanical stirring both favor a shallower MLD, leading to a very consistent projected MLD shoaling in the northern AS ($15\pm 3\%$ at 95% confidence level for RCP8.5 MMM, Figs. 3b,d). As expected, the amplitude of this shoaling correlates reasonably well ($r=0.65$) with the amplitude of the wind reduction over the northern AS (Fig. S4b).

The bias correction approach described in the previous section (i.e. correcting the projected response on the basis of AS wind speed bias) when applied to the HFlx and MLD yields a very consistent reduction across all models (Figs. 3c,d), with RCP8.5 MMM $10\pm 5\%$ and $11\pm 2\%$, respectively. As for the wind speed, the HFlx and MLD are also overestimated in CMIP5 (not shown). The reduction in HFlx and MLD responses remain robust even when performing the correction on the basis of their respective biases ($8\pm 5\%$ and $13\pm 3\%$, respectively), which will account for the potential non-linearities (not shown).

3.3 Mechanisms

In this section, we discuss the possible mechanisms responsible for the reduced IWM circulation in response to the anthropogenic global warming.

The winter monsoon arises from an interhemispheric SLP gradient, which constrains the surface winds through geostrophy. The IWM winds are clearly associated with a high pressure over the Arabian Peninsula and a low pressure below the ITCZ around $5-10^\circ\text{S}$ (Fig. S6), with frictional effects in the surface layer contributing to a veering towards low-pressure area relative to isobars in the northern hemisphere [e.g. chapter 9.2 in Gill, 1982]. As a result, the present-day (HIST) AS wind speed has a 0.71 correlation with HIST interhemispheric SLP gradient between the Arabian

Peninsula and the southern Indian Ocean (Fig. 4a; see Fig. S7a for a justification of the two selected boxes to calculate the interhemispheric SLP gradient). This interhemispheric SLP gradient is itself strongly correlated ($r=-0.69$) with the interhemispheric T_{surf} gradient (Figs. 4b, S6). Overall, in present-day climate, CMIP5 models with a larger T_{surf} contrast between the cold Arabian Peninsula and warmer southern IO in winter have a stronger interhemispheric SLP gradient and stronger winter AS surface winds (Figs. 4a,b). We now investigate these relationships in the context of projected climate change.

Figures 4c,d displays the MMM future T_{surf} and SLP changes. SLP increases over the southern IO and decreases over the Arabian Peninsula, northern AS and western India (Fig. 4d). Consequently, the interhemispheric SLP gradient reduces, resulting in a weakening of the IWM winds. There is indeed a 0.59 cross-model correlation (significant at the 99% level) between the projected AS winter wind speed and interhemispheric SLP gradient changes (Fig. 4e; Fig. S7b justifies the selection of the two boxes).

This interhemispheric SLP change is related to an interhemispheric T_{surf} change. Under a warming scenario, land warms much more than the ocean (Fig. 4c) [Joshi *et al.*, 2008; Dommenget, 2009; Boer, 2011]. This results in a projected 1 to 2.5°C decrease of the interhemispheric T_{surf} contrast in CMIP5 models (Fig. 4f). The faster land warming is not related to the lower heat capacity of the land, rather to the larger lapse rate over the land, as the troposphere over the land generally is drier than that over the oceans [e.g. Joshi *et al.*, 2008]. The upper tropospheric warming is relatively uniform in the tropics [e.g. Sobel *et al.*, 2001]: a larger lapse rate hence yields a larger surface warming over land, in particular in dry areas. This explains the relatively large warming over the dry Arabian Peninsula and Thar desert, and weaker warming over the southern IO. The SLP change in general mirrors the T_{surf} change (Figs. 4c,d). In particular, the projected changes in interhemispheric T_{surf} and SLP gradients are highly correlated ($r=-0.72$ significant at the 99% level; Fig. 4f). Overall, the CMIP5 models with the larger Arabian Peninsula warming relative to the southern IO are those with the stronger interhemispheric SLP gradient and more weakening in the AS wind speed.

Although there is a relatively good agreement between SLP and T_{surf} changes, they do not match perfectly (Figs. 4c,d). Bayr and Dommenget [2013] have indeed shown that the SLP response to global warming is much more closely related to the average tropospheric (1000 to 100hPa) temperature than to T_{surf} (because of the hydrostatic relation). There is however a relatively strong control of T_{surf} on SLP, as illustrated by the relatively high correlation between the interhemispheric T_{surf} and SLP changes (Fig. 4f). Indeed, as the tropical tropospheric temperature is

nearly uniform at higher levels [e.g. *Bayr and Dommenget, 2013*], most of the warming differences occur at lower levels. The near-surface warming is largely driven by the near-surface humidity content [e.g. *Bayr and Dommenget, 2013*] that exerts a strong control on the average tropospheric temperature, and hence on SLP.

While our study focuses on the projected wind changes, we also briefly assess the projected rainfall changes (Figs. S3b,d). Despite a decrease in the winter monsoon winds, the projected winter rainfall (Figs. S3b,d) increases under the intertropical convergence zone. As noted by Held and Soden [2006], the tropospheric warming induced by climate change results in increased water vapor concentrations owing to the Clausius-Clapeyron relation, and hence to enhanced moisture convergence. This effect probably overcomes that of the weaker horizontal circulation (which diminishes the moisture convergence), leading to increased rainfall. We however note that there are uncertainties in the projected regional rainfall in CMIP models [e.g. *Hwang and Frierson, 2013*; *Sabeerali et al., 2015*] and that these rainfall projections should hence be taken cautiously.

4. Summary and discussion

Our results indicate a robust reduction of the IWM wind intensity in CMIP5 models (Fig. 1), comparable to the wind intensity changes associated with the poleward shift of the monsoon jet in summer (Figs. S1b,c,d). This IWM wind reduction are related to an enhanced warming of the Arabian Peninsula relative to the southern Indian Ocean, that reduces the interhemispheric temperature and SLP gradients. Compared with its summer counterpart, a few studies have discussed the future changes of the winter monsoon in the Asian sector (see review by *Kitoh [2017]*), largely focusing on the East Asian region. CMIP simulations generally project a weakening (strengthening) of the East Asian winter monsoon circulation north (south) of 25°N, as a result of a northward shift of the Aleutian low and decreased northwest-southeast thermal and SLP differences across northeast Asia [e.g. *Jiang and Tian, 2013*]. These simulations also project a rainfall increase related to the southeast Asian winter monsoon in response to cyclonic wind anomalies over the south China Sea [*Siew et al., 2014*]. Although evident in some of the analyses dedicated to East Asian winter monsoon projections (e.g. Fig. 7 from *Ogata et al. [2014]* and Fig. 8 from *Kitoh [2017]*), this study is the first to discuss the projected decrease of the IWM circulation over the AS and the driving mechanisms. While both summer and winter Indian monsoonal circulation slowdown in CMIP models have been tracked back to changes in meridional temperature gradients between the IO and the northern IO landmass, the key continental regions involved differ substantially, with the summer monsoon involving temperature changes over the Tibetan Plateau [e.g. *Sooraj et al., 2015*] and winter monsoon being mainly influenced by temperature and SLP changes over the Arabian

Peninsula and the Thar desert.

The projected AS weakening discussed here is stronger (-0.38 ms^{-1} / -6.5% ; RCP8.5) than the general reduction of tropical surface wind speed (-0.15 ms^{-1} / -2.6% ; RCP8.5) discussed by *Held and Soden* [2006]. Both these reductions are however moderately correlated ($r=0.48$, $p=0.95$) across the models. This may be due to a common underlying mechanism [*Bayr and Dommenges*, 2013], in which the lower tropospheric humidity constrain the amplitude of the tropospheric warming and SLP change, and hence that of the circulation change.

The expected decrease of the ISM circulation depicted in CMIP models can already be detected in observations over the last half-century [*Fan et al.*, 2010]. In contrast, there is no consistent trend in the observed winds over the AS region in winter (Fig. S8e). The decreasing trend detected by CMIP models is however entirely within the range of the model's internal variability until the year 2030 (Figs. S8a,c for RCP8.5 and Figs. S8b,d for 4.5), which explains why such a trend is not yet detectable in observations. The projected AS wind speed by 2100 is 2.2 ± 0.3 (1.2 ± 0.2) times larger than the present-day internal non-seasonal, and hence interannual, variability in RCP8.5 (RCP4.5).

The increased winter rainfall over the equatorial IO has implications for regional water resources. The projected rainfall increase is significant mostly over the ocean, but may be socio-economically relevant for the east African countries and the islands located in the equatorial IO. In contrast, the rainfall change over southern India and Sri Lanka is not statistically significant. The projected changes in regional rainfall are however highly sensitive to CMIP model biases [e.g. *Hwang and Frierson*, 2013; *Sabeerali et al.*, 2015], and hence need further assessment..

These IWM circulation changes are potentially important for the AS biogeochemistry. Previous studies have mainly focused on summer AS productivity, with some of them suggesting a decline due to increased thermal stratification [*Roxy et al.*, 2015] while the others suggesting an increase due to a poleward shift of the monsoon jet [*Praveen et al.*, 2016]. The northern AS winter bloom contributes significantly to the annual AS productivity, but its response to climate change has so far not been discussed. This bloom is largely the result of the convective entrainment of nutrients into the mixed layer during winter [e.g. *Prasanna Kumar et al.*, 2001; *Keerthi et al.*, 2016]. The projected weakening of the winter AS winds will reduce the oceanic stirring (Fig. S5) and heat losses (Figs. 3ac) to the atmosphere over the northern part of the basin. This will in turn reduce the winter mixed layer deepening (Figs. 3bd) and hence the amount of nutrients entraining into the mixed layer, leading to a possible reduction in the AS productivity during winter. The winter convective

overturning not only influences the AS productivity but also ventilates the upper boundary of the AS oxygen minimum zone [Morrison *et al.*, 1999], which is one of the most intense in the world oceans. The reduced winter ventilation may further contribute to the projected expansion of the AS oxygen minimum zone in the future [Bopp *et al.*, 2013]. These issues will be addressed in a future study.

Acknowledgements

We thank Director, CSIR-NIO for his support. This work was done while ML and TI were visiting scientists at the CSIR-National Institute of Oceanography (CSIR-NIO) under Institut de Recherche pour le Développement (IRD) funding. JV acknowledges IRD for supporting regular visits to CSIR-NIO and thanks CSIR-NIO for his “Adjunct Scientist” position. IS acknowledges financial support from CSIR, New Delhi and INCOIS/MoES (HOOFS project). PV is funded through a CSIR Senior Research Fellow grant and thanks Hema Naik for her support. We acknowledge the World Climate Research Program's Working Group on Coupled Modelling, which is responsible for CMIP, and we thank the climate modeling groups (listed in Table ST1) for producing and making available their model outputs. All the CMIP5 model outputs were downloaded from the Institut Pierre Simon Laplace (IPSL) CCIPLAD repository. This is NIO contribution XXXX.

References

- Banse, K., and C. R. McClain (1986), Winter blooms of phytoplankton in the Arabian Sea as observed by the coastal zone colour scanner, *Marine Ecology-Progressive Series* 34, 201-211.
- Bayr, T., and D. Dommenges (2013), The tropospheric land-sea warming contrast as the driver of tropical sea level pressure changes, *J. Climate*, 26, 1387-1402.
- Boer, G. J. (2011), The ratio of land to ocean temperature change under global warming, *Climate Dynam.*, 37(11–12), 2253–2270.
- Bopp, L., L. Resplandy, J. C. Orr, S. C. Doney, J. P. Dunne, M. Gehlen, P. Halloran, C. Heinze, T. Ilyina, R. Séférian, J. Tjiputra, and M. Vichi (2013), Multiple stressors of ocean ecosystems in the 21st century: projections with CMIP5 models, *Biogeosciences*, 10, 6225–6245.
- Bracegirdle, T. J., and D. B. Stephenson (2012), Higher precision estimates of regional polarwarming by ensemble regression of climate model projections, *Clim. Dyn.*, 39, 2805–2821.
- Bracegirdle, T. J., and D.B. Stephenson (2013), On the Robustness of Emergent Constraints Used in Multimodel Climate Change Projections of Arctic Warming, *J. Climate*, 26, 669–678.
- Christensen, J. H., K. Krishna Kumar, E. Aldrian, S.-I. An, I. F. A. Cavalcanti, M. de Castro, W. Dong, P. Goswami, A. Hall, J. K. Kanyanga, A. Kitoh, J. Kossin, N.-C. Lau, J. Renwick, D. B. Stephenson, S.-P. Xie and T. Zhou (2013), Climate phenomena and their relevance for future regional climate change, *Climate Change 2013, The Physical Science Basis. Contribution of Working Group I to the Fifth Assessment Report of the Intergovernmental Panel on Climate Change*. Stocker, T. F., D. Qin, G.-K. Plattner, M. Tignor, S. K. Allen, J. Boschung, A. Nauels, Y. Xia, V. Bex and P. M. Midgley (eds.) Cambridge University Press, Cambridge, United Kingdom and New York, NY, USA.
- Cox, P. M., D. Pearson, B. B. Booth, P. Friedlingstein, C. Huntingford, C. D. Jones, and C. M. Luke (2013), Sensitivity of tropical carbon to climate change constrained by carbon dioxide variability, *Nature*, 494(7437), 341–344.

- de Boyer Montégut, C., G. Madec, A. S. Fischer, A. Lazar, and D. Iudicone (2004), Mixed layer depth over the global ocean: an examination of profile data and a profile-based climatology, *J. Geophys. Res.*, *109*, C12003.
- Dee, D. P., S. M. Uppala, A. J. Simmons, P. Berrisford, P. Poli, S. Kobayashi, U. Andrae, M. A. Balmaseda, G. Balsamo, P. Bauer, P. Bechtold, A. C. M. Beljaars, L. van de Berg, J. Bidlot, N. Bormann, C. Delsol, R. Dragani, M. Fuentes, A. J. Geer, L. Haimberger, S. B. Healy, H. Hersbach, E. V. Hólm, L. Isaksen, P. Kållberg, M. Köhler, M. Matricardi, A. P. McNally, B. M. Monge-Sanz, J.-J. Morcrette, B.-K. Park, C. Peubey, P. de Rosnay, C. Tavolato, J.-N. Thépaut, and F. Vitart (2011), The ERA-Interim reanalysis: configuration and performance of the data assimilation system, *Q.J.R. Meteorol. Soc.*, *137*, 553–597.
- Dimri, A. P., D. Niyogi, A. P. Barros, J. Ridley, U. C. Mohanty, T. Yasunari, and D. R. Sikka (2015), Western Disturbances: A review, *Rev. Geophys.*, *53*, 225–246.
- Dommenget, D. (2009), The ocean's role in continental climate variability and change, *J. Climate*, *22*, 4939–4952.
- Endo, H., and A. Kitoh (2016), Projecting Changes of the Asian Summer Monsoon Through the Twenty-First Century, In *The Monsoons and Climate Change* (pp. 47-66), Springer International Publishing.
- Fan, F., M. E. Mann, S. Lee, and J. L. Evans (2010), Observed and modeled changes in the South Asian summer monsoon over the historical period, *J. Climate*, *23*, 5193-5205.
- Findlater, J. (1971), Mean monthly airflow at low levels over the western Indian Ocean, *Geophysical Memoirs, No. 115*, HMSO, London, 53 p.
- Gadgil, S. (2003), The Indian monsoon and its variability, *Annual Review of Earth and Planetary Sciences*, *31*(1), 429-467.
- Gadgil, S. and S. Gadgil (2006), The Indian Monsoon, GDP and agriculture, *Econom. Pol. Weekly* *41*, 4887 – 4895.
- Gill, A. E. (1982), *Atmosphere-Ocean Dynamics*, 662 pp., Academic, San Diego, Calif.
- Goswami, B. N., V. Venugopal, D. Sengupta, M. Madhusoodanan, and P. K. Xavier (2006), Increasing trend of extreme rain events over India in a warming environment, *Science* *314*, 1442–1445.
- Held, I. M., and B. J. Soden (2006), Robust responses of the hydrological cycle to global warming, *J. Climate*, *19*, 5686–5699.
- Hwang, Y.-T., and D. M. W. Frierson (2013), Link between the double-Intertropical Convergence Zone problem and cloud bias over Southern Ocean, *Proc. Natl. Acad. Sci. U.S.A.*, *110*, 4935–4940, doi:10.1073/pnas.1213302110
- Jiang, D., and Z. Tian (2013), East Asian monsoon change for the 21st century: results of CMIP3 and CMIP5 models, *Chin Sci Bull* *58*(12), 1427–1435.
- Joshi, M. M., J. M. Gregory, M. J. Webb, D. M. H. Sexton, and T. C. Johns (2008), Mechanisms for the land/sea warming contrast exhibited by simulations of climate change, *Climate Dynam.*,

30(5),455–465.

- Keerthi, M. G., M. Lengaigne, M. Levy, J. Vialard, V. Parvathi, C. de Boyer Montegut, C. Ethe, O. Aumont, I. Suresh, V. P. Akhil, and P.M. Muraleedharan (2017), Physical control of interannual variations of the winter chlorophyll bloom in the northern Arabian Sea, *Biogeosciences*, 14, 3615-3632, <https://doi.org/10.5194/bg-14-3615-2017>.
- Kitoh, A. (2017), The Asian Monsoon and its Future Change in Climate Models: A Review, *Journal of the Meteorological Society of Japan. Ser. II*, 95(1), 7-33.
- Levine, R. C., A. G. Turner, D. Marathayil, and G. M. Martin (2013), The role of northern Arabian Sea surface temperature biases in CMIP5 model simulations and future projections of Indian summer monsoon rainfall, *ClimDyn* 41(1),155–172.
- Li, G., S-P. Xie, Y. Du, and Y. Luo. (2016b), Effects of excessive equatorial cold tongue bias on the projections of tropical Pacific climate change. Part I: the warming pattern in CMIP5 multi-model ensemble, *Clim.Dyn.*, 47, 3817.
- Li, G., S-P. Xie, and Y. Du (2016a), A robust but spurious pattern of climate change in model projections over the tropical Indian Ocean, *J.Clim.*, 29, 5589–5608.
- Madhupratap, M., S. Prasanna Kumar, P. M. A. Bhattathiri, M. D. Kumar, S. Raghukumar, K. K. C. Nair, and N. Ramaiah (1996), Mechanism of the biological response to winter cooling in the northeastern Arabian Sea, *Nature*, 384, pp. 549–552.
- Madhupratap, M., K. N. V. Nair, T. C. Gopalkrishnan, P. Haridas, K. K. C. Nair, and P. Venugopal (2001), Arabian Sea oceanography and fisheries of the west coast of India, *Current Sci.*, 81, 355–361.
- Marathayil, D., A. G. Turner, L. C. Shaffrey, and R. C. Levine (2013), Systematic winter sea-surface temperature biases in the northern Arabian Sea in HiGEM and the CMIP3 models, *Environ Res Lett* 8(1), 014028.
- Marra, J., and R. T. Barber (2005), Primary productivity in the Arabian Sea: A synthesis of JGOFS data, *Progress in Oceanography*, 65(2), 159-175.
- Morrison, J. M., L. A. Codispoti, S. L. Smith, K. Wishner, C. Flagg, W. D. Gardner, S. Gaurin, S.W. A. Naqvi, V. Manghnani, L. Prosperie, and J. S. Gundersen (1999), The oxygen minimum zone in the Arabian Sea during 1995, *Deep-Sea Research II*, 46, pp. 1903–1931.
- Moss, R. H., J. A. Edmonds, K. A. Hibbard, M. R. Manning, S. K. Rose, D. P. van Vuuren, T. R. Carter, S. Emori, M. Kainuma, T. Kram, G. A. Meehl, J. F. B. Mitchell, N. Nakicenovic, K. Riahi, S. J. Smith, R. J. Stouffer, A. M. Thomson, J. P. Weyant, and T. J. Wilbanks (2010), The next generation of scenarios for climate change research and assessment, *Nature*, 463,747–756.
- Ogata, T., H. Ueda, T. Inoue, M. Hayasaki, A. Yoshida, S. Watanabe, M. Kira, M. Ooshiro, and A. Kumai (2014), Projected future changes of the Asian Monsoon: A Comparison of CMIP3 and CMIP5 model results, *J. Meteorol. Soc. Japan* 92, 207–225.
- Prasanna Kumar, S., N. Ramaiah, M. Gauns, V. V. S. S. Sarma, P. M. Muraleedharan, S. Raghukumar, M. D. Kumar, and M. Madhupratap (2001), Physical forcing of biological

productivity in the northern Arabian Sea during the Northeast Monsoon, *Deep Sea Res., Part II*, 48(6–7), 1115–1126.

- Praveen, V., R. S. Ajayamohan, V. Valsala, and S. Sandeep (2016), Intensification of upwelling along Oman coast in a warming scenario, *Geophys. Res. Lett.*, 43, doi:10.1002/2016GL069638.
- Praveen Kumar, B., J. Vialard, M. Lengaigne, V. S. N. Murty, and M. McPhaden (2012), TropFlux: air-sea fluxes for the global tropical oceans: description and evaluation, *Clim. Dyn.*, 38(7–8), 1521–1543.
- Rajeevan, M., C.K. Unnikrishnan, J. Bhate, K. Niranjan Kumar, and P.P. Sreekala (2012), Northeast monsoon over India: variability and prediction. *Met. Apps.*, 19, 226–236.
- Roxy, M. K., K. Ritika, P. Terray, R. Murtugudde, K. Ashok, and B. N. Goswami (2015), Drying of Indian subcontinent by rapid Indian Ocean warming and a weakening land-sea thermal gradient, *Nat. Commun.*, 6, 7423.
- Sabeerali, C.T., S.A. Rao., A.R. Dhakate, K. Salunke, and B.N. Goswami (2015), Why ensemble mean projection of south Asian monsoon rainfall by CMIP5 models is not reliable?, *Clim. Dyn.*, 45 (1-2), 161-174.
- Saji, N. H., B. N. Goswami, P. N. Vinayachandran, and T. Yamagata (1999), A dipole mode in the tropical Indian Ocean, *Nature*, 401, 360–363.
- Sandeep, S., and R. S. Ajayamohan (2015), Poleward shift in Indian summer monsoon low level jetstream under global warming, *Clim. Dyn.*, 45, 337–351.
- Sandeep, S., and R. S. Ajayamohan (2014), Origin of cold bias over the Arabian Sea in climate model, *Sci. Rep.*, 4, 6403.
- Sharmila, S., S. Joseph, A. K. Sahai, S. Abhilash, and R. Chattopadhyay (2015), Future projection of Indian summer monsoon variability under climate change scenario: An assessment from CMIP5 climate models. *Global Planet. Change*, 124, 62-78.
- Siew, J. H., F. T. Tangang, and L. Juneng (2014), Evaluation of CMIP5 coupled atmosphere-ocean general circulation models and projection of the Southeast Asian winter monsoon in the 21st century. *Int. J. Climatol.*, 34, 2872-2884.
- Smith, S.L., and M. Madhupratap (2005), Mesozooplankton of the Arabian Sea: Patterns influenced by seasons, upwelling, and oxygen concentrations, *Progress in Oceanography*, 65, 214-239.
- Sobel, A. H., J. Nilsson, and L. M. Polvani (2001). The weak temperature gradient approximation and balanced tropical moisture waves. *J. Atmos. Sci.*, 58, 3650-3665.
- Sooraj, K. P., P. Terray, and M. Mujumdar (2015), Global warming and the weakening of the Asian summer Monsoon circulation: assessments from the CMIP5 models, *Clim. Dyn.* 45, 1–20.
- Sperber, K. R., H. Annamalai, I. S. Kang, A. Kitoh, A. Moise, A. Turner, B. Wang, and T. Zhou (2013), The Asian summer monsoon: an intercomparison of CMIP5 vs. CMIP3 simulations of the late 20th century, *Clim Dyn* 41(9–10), 2711–2744.
- Trenberth, K. E., D. P. Stepaniak, and J. M. Caron (2000), The global monsoon as seen through the

divergent atmospheric circulation. *Journal of Climate*, 13(22), 3969-3993.

Turner, A. G., and H. Annamalai (2012), Climate change and the South Asian summer monsoon, *Nat. Clim. Change* 2, 587–595.

Vialard, J., P. Terray, J. P. Duvel, R. S. Nanjundiah, S. S. C. Shenoi, and D. Shankar (2011), Factors controlling January–April rainfall over southern India and Sri Lanka. *Climate dynamics*, 37(3-4), 493-507.

Webster, P. J., V. O. Magana, T. N. Palmer, T. A. Tomas, M. Yanai, and T. Yasunari (1998), Monsoons: Processes, predictability, and prospects for prediction, *J. Geophys. Res.*, 103, 14 451–14 510.

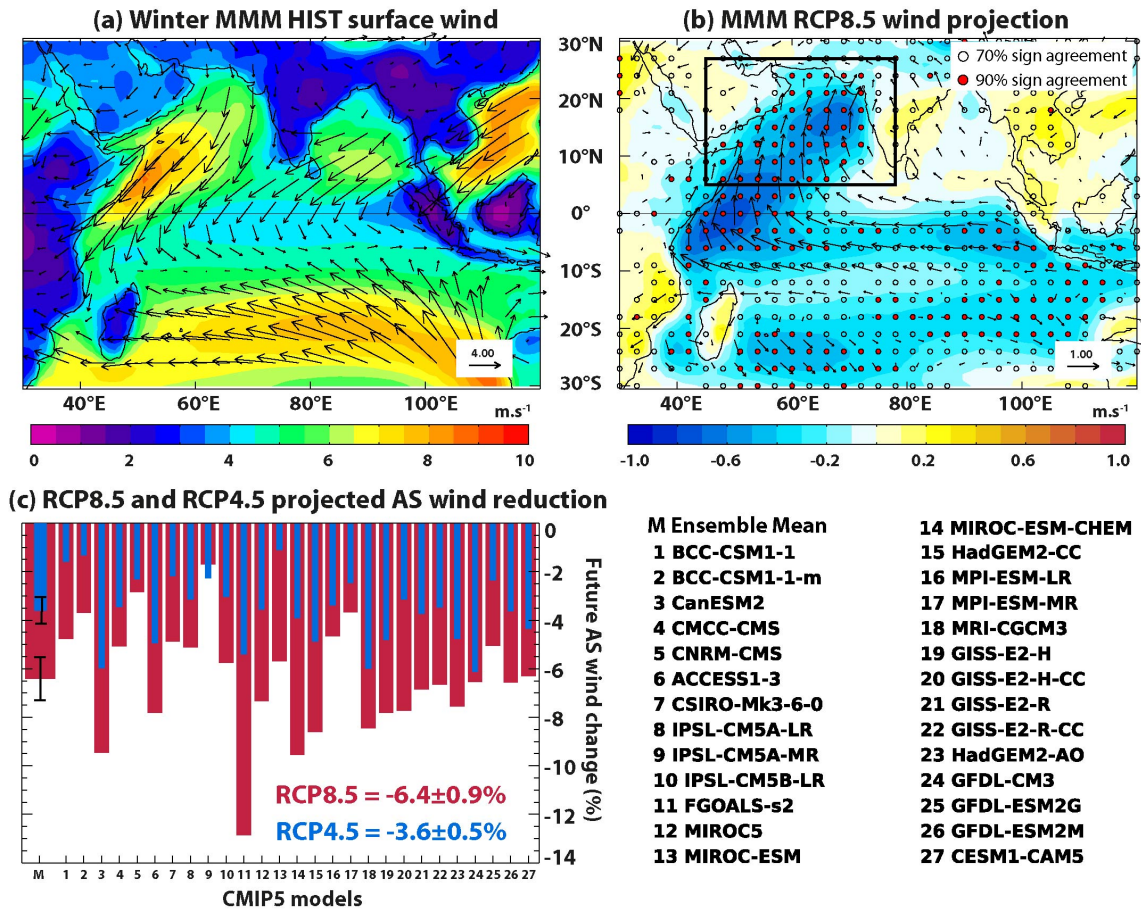


Figure 1. Multi Model Mean (MMM) winter (DJFM) climatology of surface winds (vectors) and speed (color) for **(a)** present-climate (HIST) and **(b)** RCP8.5 projected changes. Regions where more than 70% (90%) models agree on the sign of the wind speed change are indicated with black circle (red dots) on panel b. **(c)** Bar plot of the percentage of projected surface wind speed changes in RCP8.5 (red) and RCP4.5 (blue) scenarios in winter within the AS (black frame on panel b) for individual models and MMM with black whiskers indicating the 95% confidence interval (values indicated) on the mean. The models used in the present study (with model IDs) are listed in the bottom right panel.

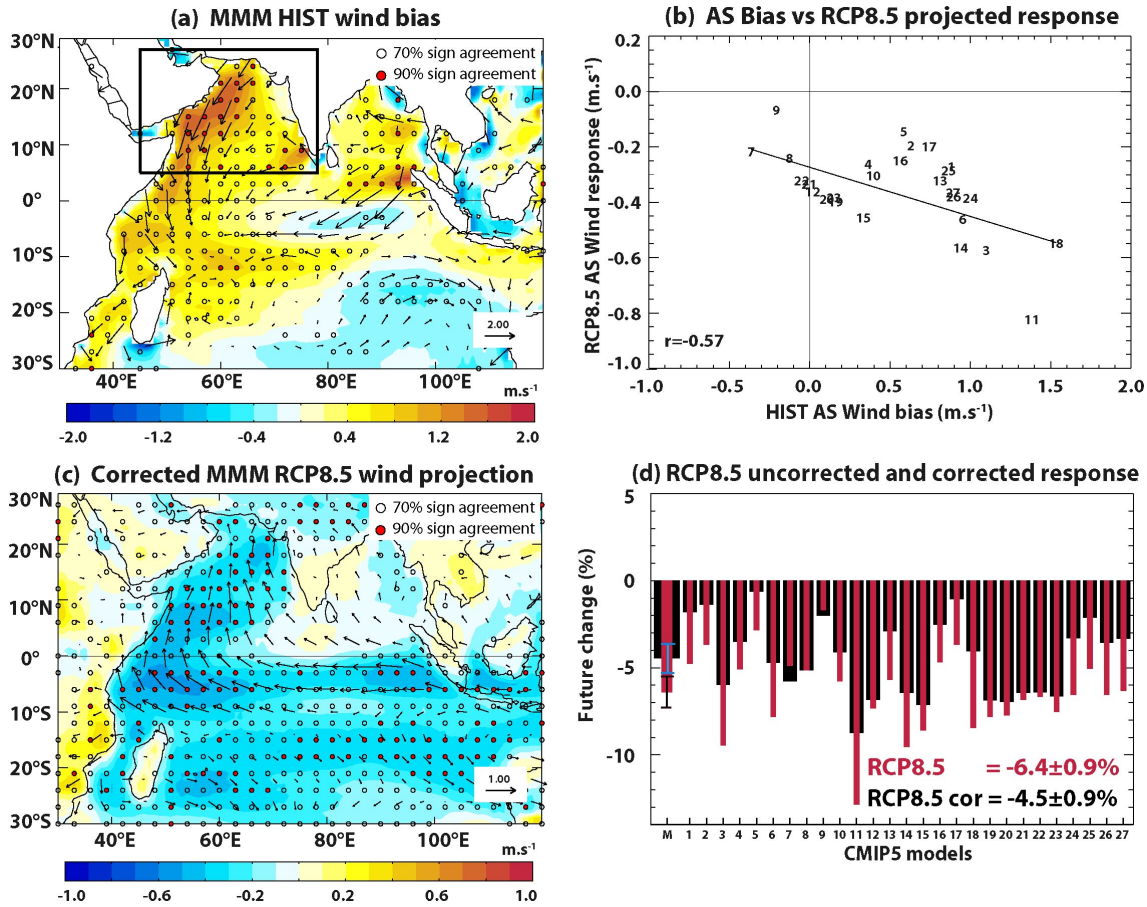


Figure 2. (a) Multi Model Mean (MMM) bias in the winter wind speed climatology relative to the Tropflux dataset. (b) Scatter plot of average AS winter wind speed bias versus RCP8.5 wind speed projected change for individual models (see Fig. 1 for model IDs). The regression line and correlation value are also shown. (c) MMM RCP8.5 projected winter bias corrected (see text and supporting information for details) wind speed changes. (d) Bar plot of the percentage of future RCP8.5 surface wind speed corrected (black) and uncorrected (red) changes in the AS (black frame on panel a) for individual models and MMM with whiskers indicating the 95% confidence interval (values indicated) on the mean. Regions where more than 70% (90%) models agree on the sign of the wind speed bias/changes are indicated with black circle (red dots) on panels a/panel c.

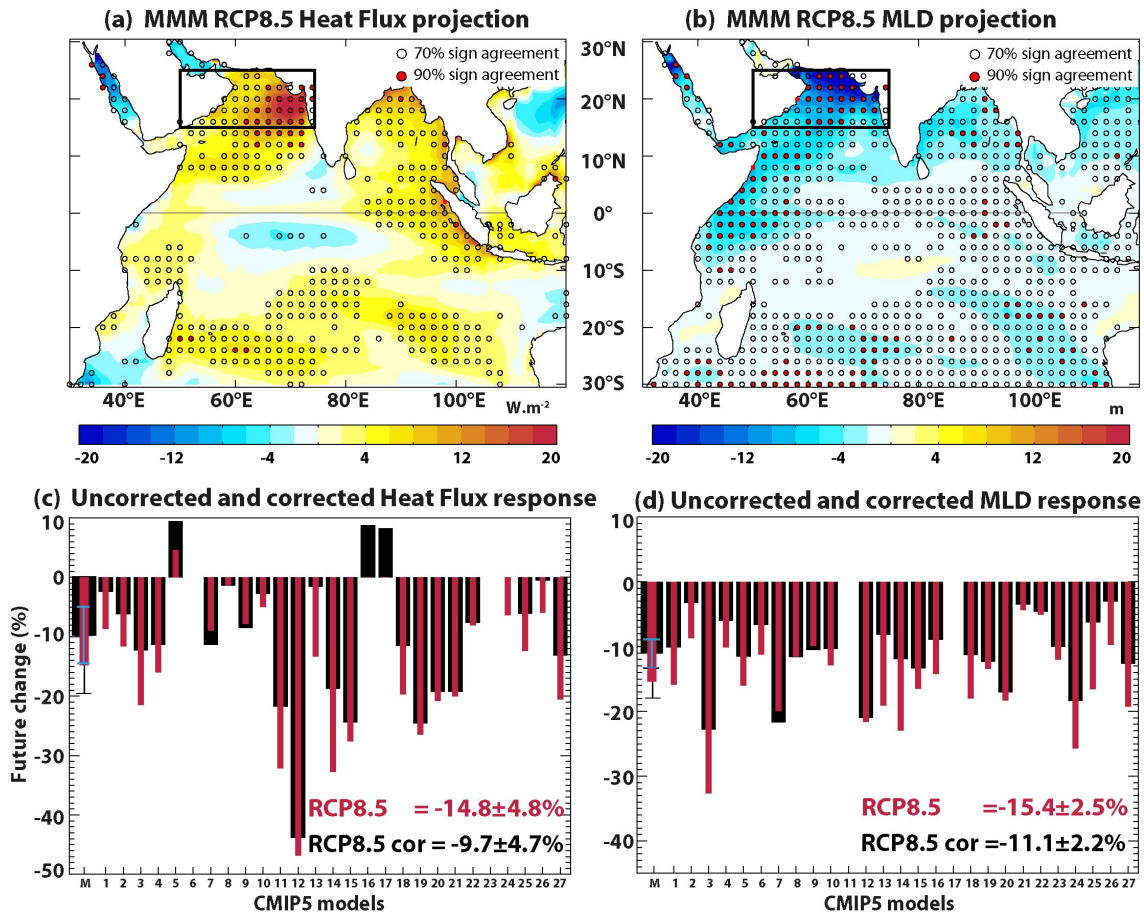


Figure 3. Multi Model Mean (MMM) winter RCP8.5 (a) net heat flux (HFlx) and (b) MLD projected changes. Regions where more than 70% (90%) models agree on the sign of the change are indicated with black circle (red dots) on panels a and b. Bar plots of the percentage of future RCP8.5 (c) HFlx and (d) MLD corrected and uncorrected changes in the northern AS box (black frame on panels a and b) for individual models and MMM with whiskers indicating the 95% confidence interval (values indicated) on the mean.

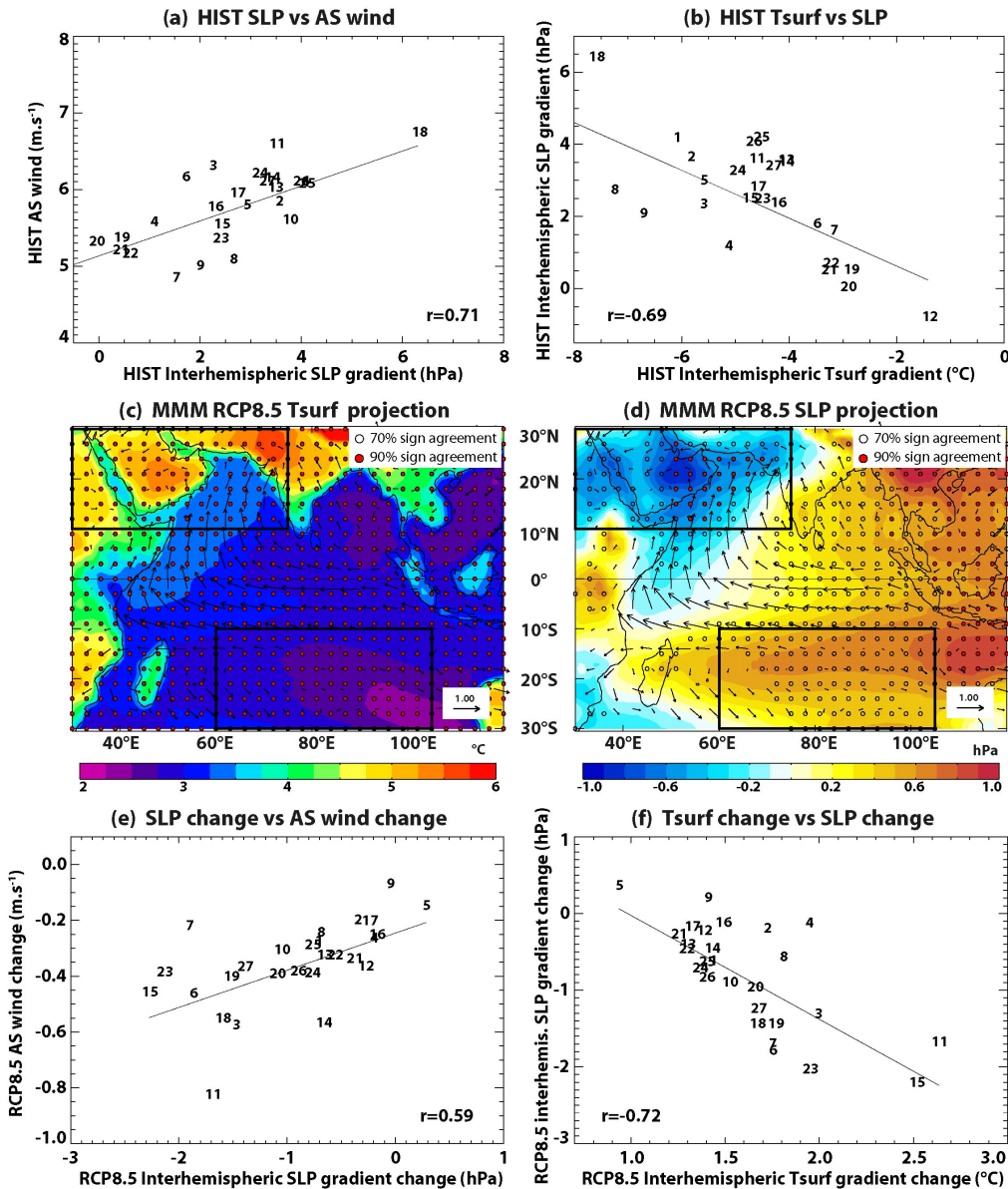


Figure 4. Scatterplots of present-day (HIST) interhemispheric sea level pressure gradient against (a) HIST AS wind speed (box shown on Fig. 1b) and (b) HIST land-sea interhemispheric surface temperature (Tsurf) gradient for individual models. Interhemispheric gradients are calculated as the difference between the averaged values over boxes (north minus south) shown on panels c,d. Multi Model Mean (MMM) winter climatology of RCP8.5 projected changes for (c) Tsurf (°C) and (d) mean sea level pressure (hPa; SLP) with wind changes overlaid as vectors. Regions where more than 70% (90%) models agree on the sign of the change are indicated with black circle (red dots) on both panels. Scatterplot of RCP8.5 projected interhemispheric SLP gradient changes against (e) wind speed changes in the AS (box on Fig. 1b) and (f) interhemispheric land-sea Tsurf gradient changes. See Fig. 1 for model ID for each model on scatterplots. The regression lines and correlation values are also shown on panels a, b, e, and f.

Robust projected weakening of winter monsoon winds over the Arabian Sea under climate change

V. Parvathi¹, I. Suresh¹, M. Lengaigne^{2,3}, T. Izumo^{2,3}, J. Vialard²

¹ CSIR-National Institute of Oceanography (CSIR-NIO), Goa, India

² Sorbonne Universités (UPMC, Univ Paris 06)-CNRS-IRD-MNHN, LOCEAN Laboratory, IPSL, Paris, France

³ Indo-French Cell for Water Sciences, IISc-NIO-IITM-IRD Joint International Laboratory, NIO, Goa, India

Contents of this file

Supplementary table ST1

Supplementary figures S1 to S8

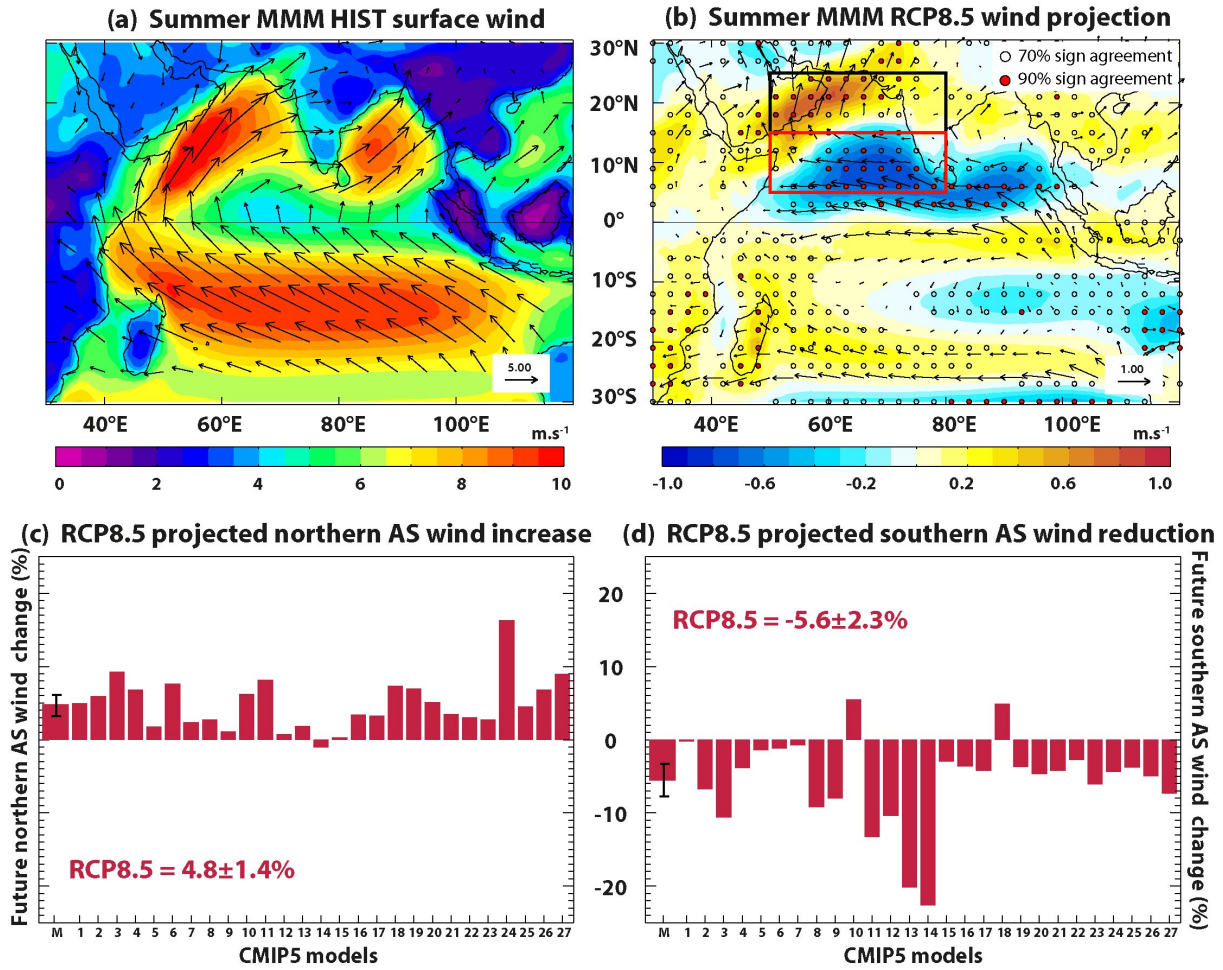
Details on the bias correction method used in the manuscript.

Purpose of each supplementary figure and table

Table ST1 lists the CMIP models used in this study, and also lists the available variables for each model. Figure S1 allows to compare the present-day and the projected RCP8.5 AS wind changes in summer with those in winter shown in Figure 1. Figure S2 shows the bias corrected wind changes under RCP4.5 (i.e. same as Figure 2, but for RCP4.5). Figure S3 shows the projected rainfall anomalies in summer and winter (RCP8.5 scenario). Figure S4 links the changes of surface net HFlx and MLD in the Northern AS to those of winds. Figure S5 shows the present-day climatology and projected changes of AS wind stress. Figure S6 shows the present-day MMM SLP and Tsurf in the HIST. Figure S6 shows the large-scale pattern of SLP associated with present-day and projected RCP8.5 winter AS wind changes. Figure S8 shows time-series of past and projected AS wind speed changes in CMIP5 (both RCP8.5 and 4.5) and in observations.

Model ID	Model name	SfcWind	TS	SLP	NetFlux	MLD	Wind stress
1	BCC-CSM1-1						
2	BCC-CSM1-1-M						
3	CanESM2						
4	CMCC-CMS						
5	CNRM-CM5						
6	ACCESS1-3						
7	CSIRO-Mk3-6-0						
8	IPSL-CM5A-LR						
9	IPSL-CM5A-MR						
10	IPSL-CM5B-LR						
11	FGOALS-s2						
12	MIROC5						
13	MIROC-ESM						
14	MIROC-ESM-CHEM						
15	HadGEM2-CC						
16	MPI-ESM-LR						
17	MPI-ESM-MR						
18	MRI-CGCM3						
19	GISS-E2-H						
20	GISS-E2-H-CC						
21	GISS-E2-R						
22	GISS-E2-R-CC						
23	HadGEM2-AO						
24	GFDL-CM3						
25	GFDL-ESM2G						
26	GFDL-ESM2M						
27	CESM1-CAM5						

Table ST1: List of CMIP5 models used in this study, with color shading on a cell indicating the availability of parameters (white when not available). The Model IDs are used to identify each model in all scatterplots.



FigureS1.(a,b) As Figure 1a,b for summer (JJAS). Bar plots of the percentage of projected RCP8.5 surface wind speed change in summer within (c) the northern AS and (d) southern AS boxes (depicted as black and red frames on panel b) for individual models and MMM with black whiskers marking 95% confidence interval (values indicated) on the mean.

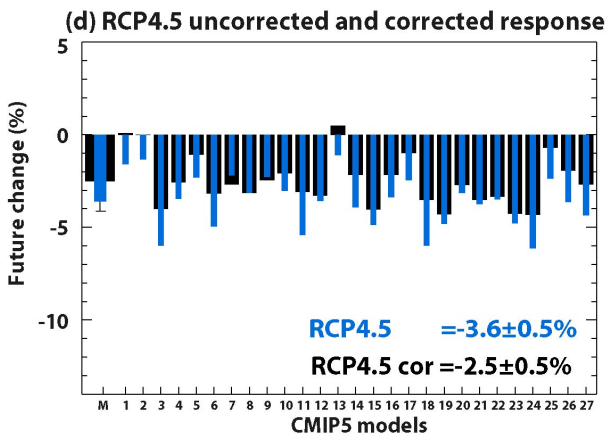
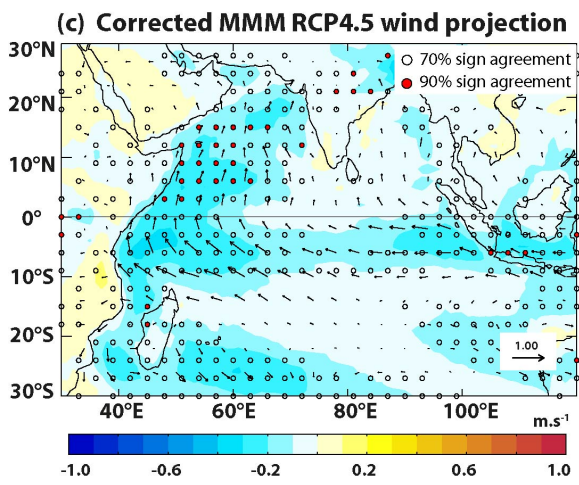
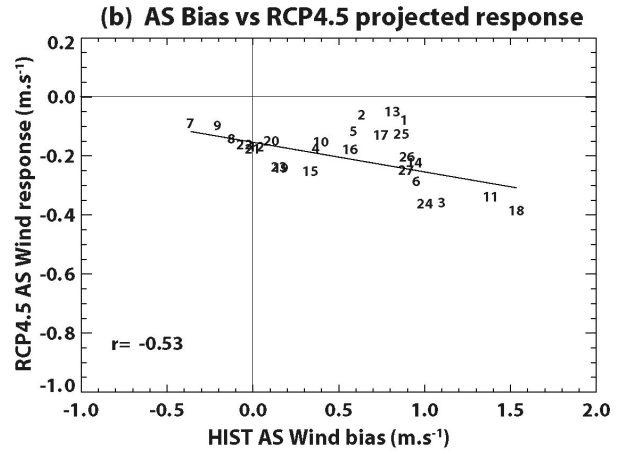
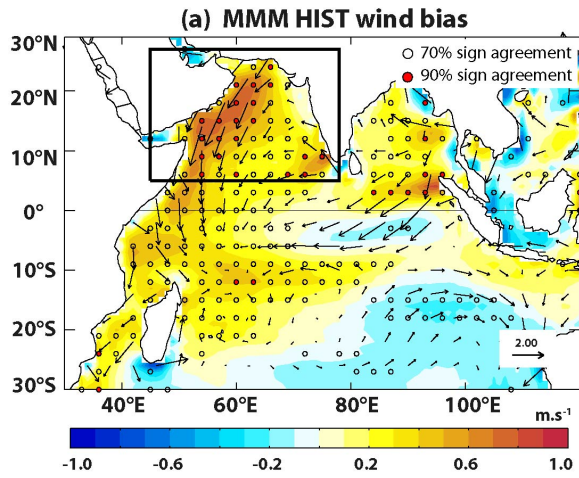


Figure S2.As Figure 2, but for RCP4.5 scenario.

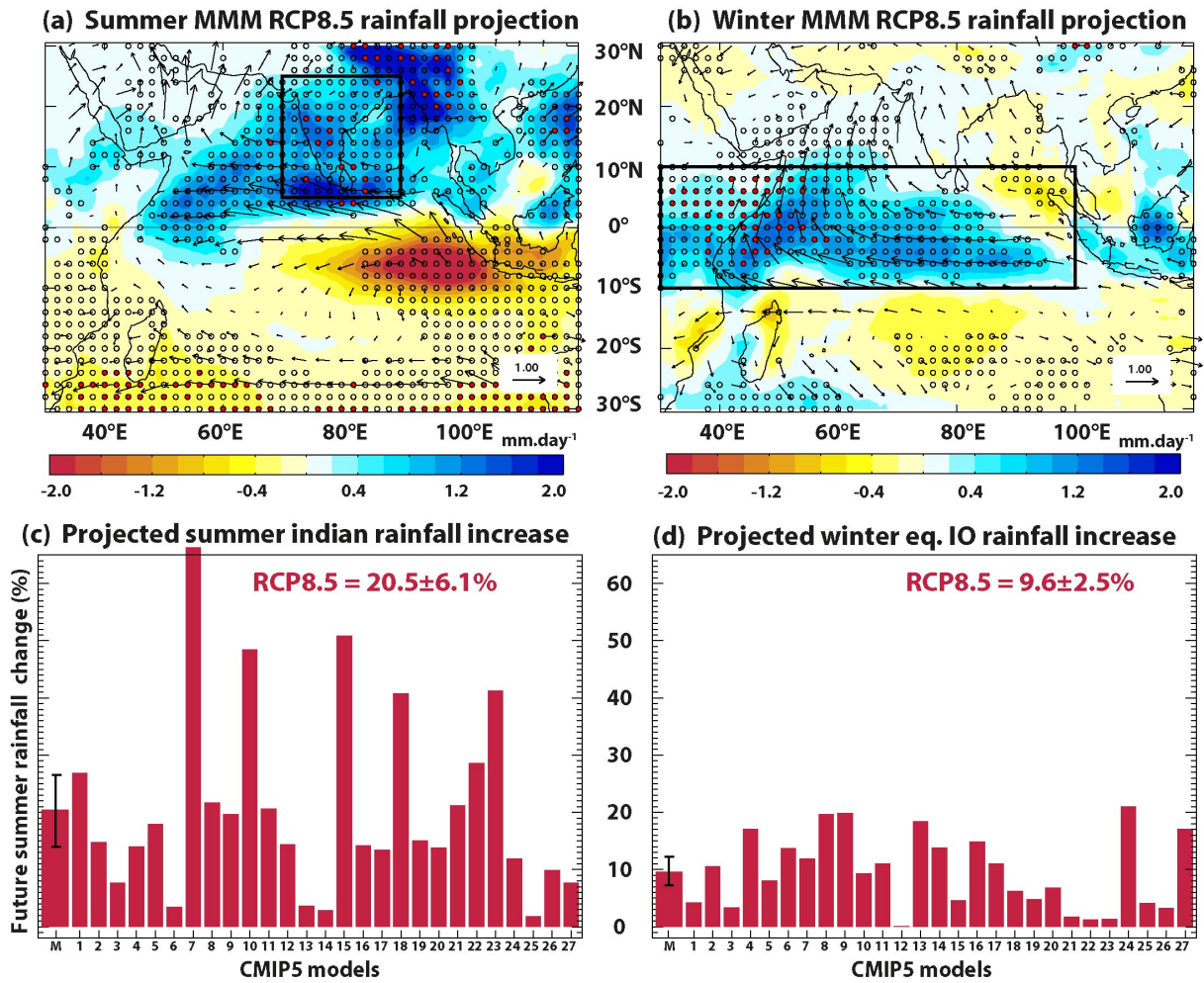
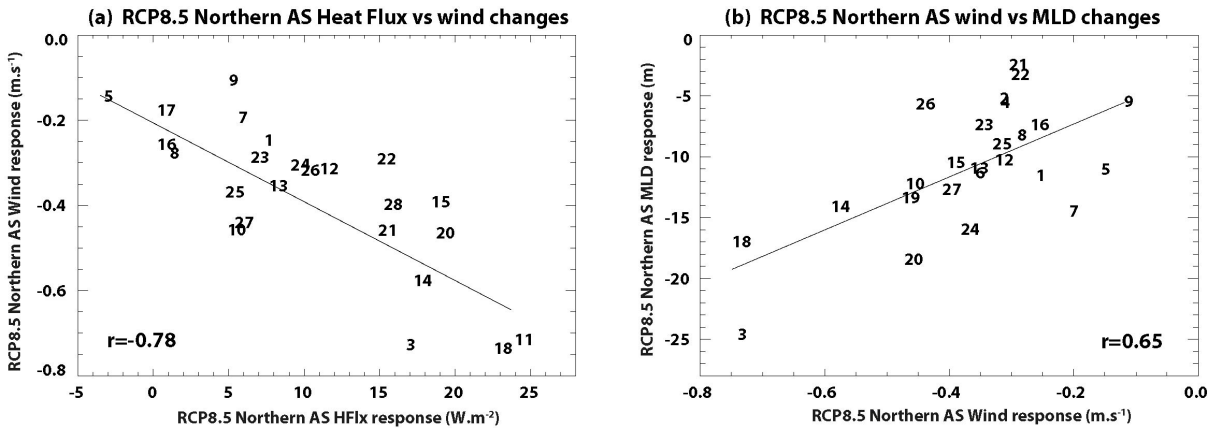
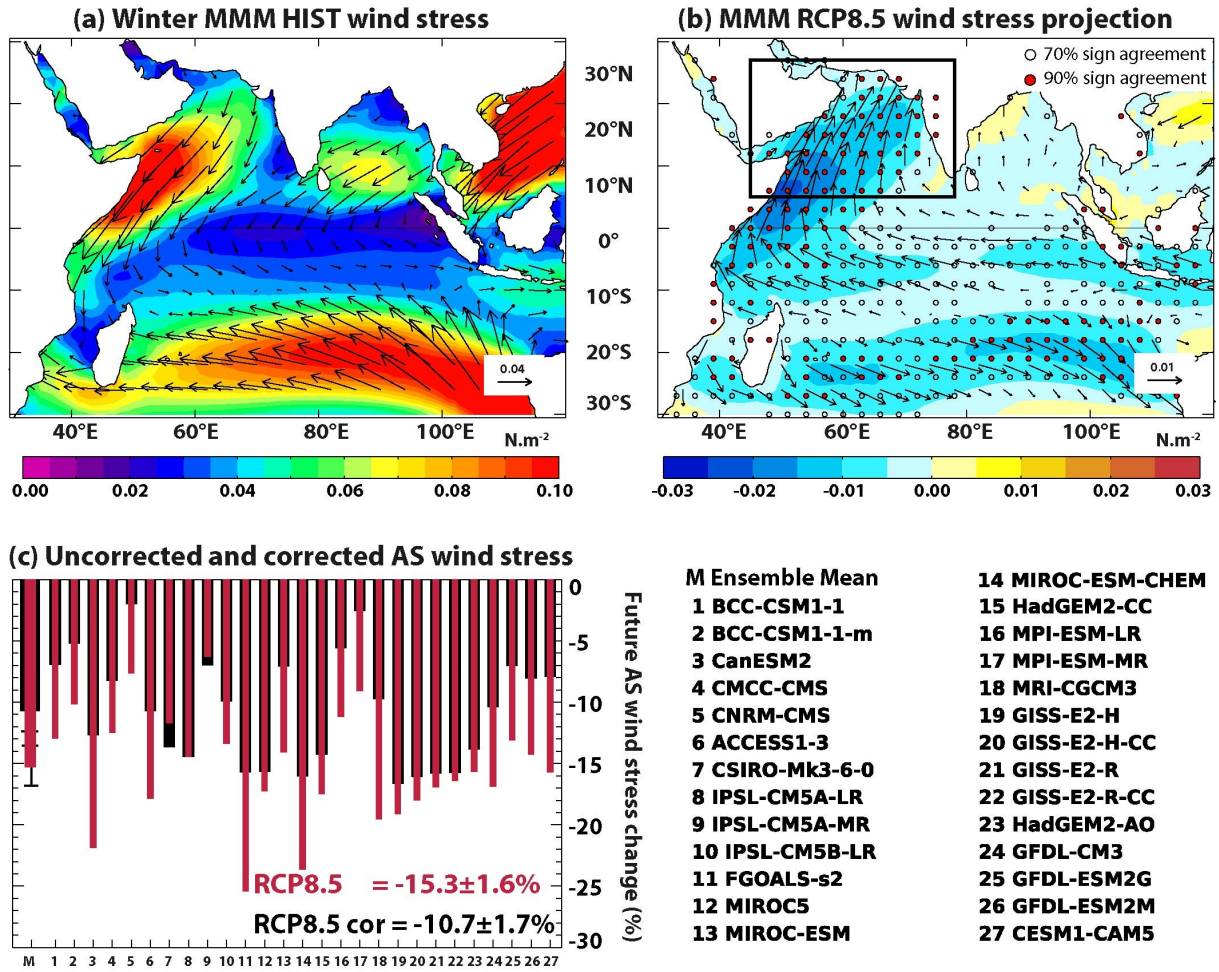


Figure S3. Projected RCP8.5 MMM precipitation (color) and wind speed (vector) changes for **(a)** summer (JJAS) and **(b)** winter (DJFM). Regions where more than 70% (90%) models agree on the sign of the wind speed change are indicated with empty black (filled red) dots on panels a and b. Bar plots of the percentage of projected RCP8.5 precipitation changes over **(c)** the Indian subcontinent region in summer and **(d)** the equatorial IO region in winter (depicted as black frames on panel a and b) for individual models and for the MMM, with black whiskers marking 95% confidence interval (values indicated on the panels).



FigureS4. (a) Scatterplots of RCP8.5 projected average northern AS (black frames on Figure 3a,b) winter wind speed changes against those of (a)HFlx and (b) MLD. Related regression lines and correlation values are provided on each panel. See table ST1 for the identifying each model by its Model ID.



FigureS5. As Figure 1, but for surface wind stress.

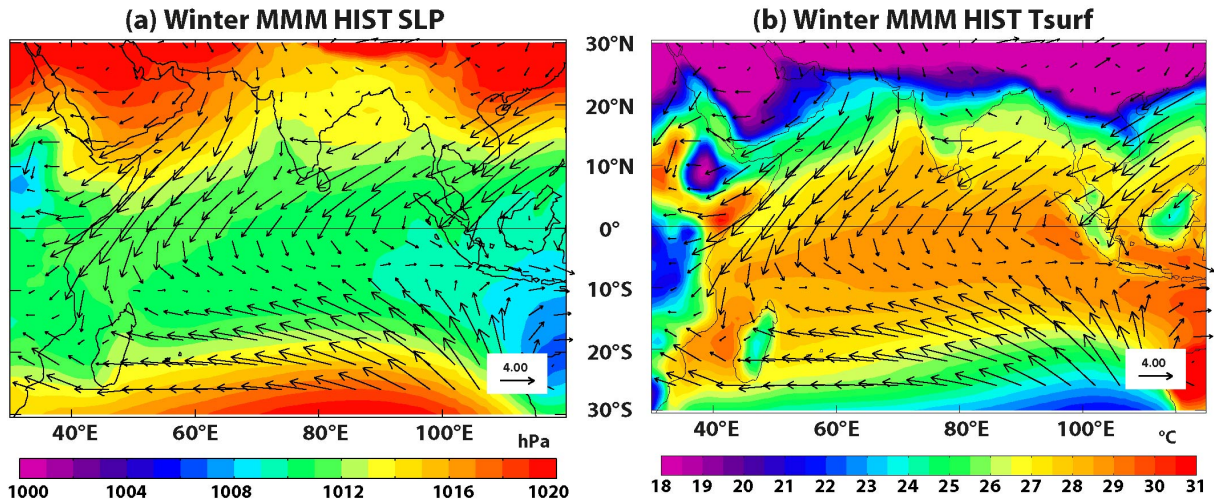


Figure S6. MMM of winter (DJFM) climatological (a) mean SLP (color) (b) mean Tsurf (color) with surface wind speed vectors overlaid.

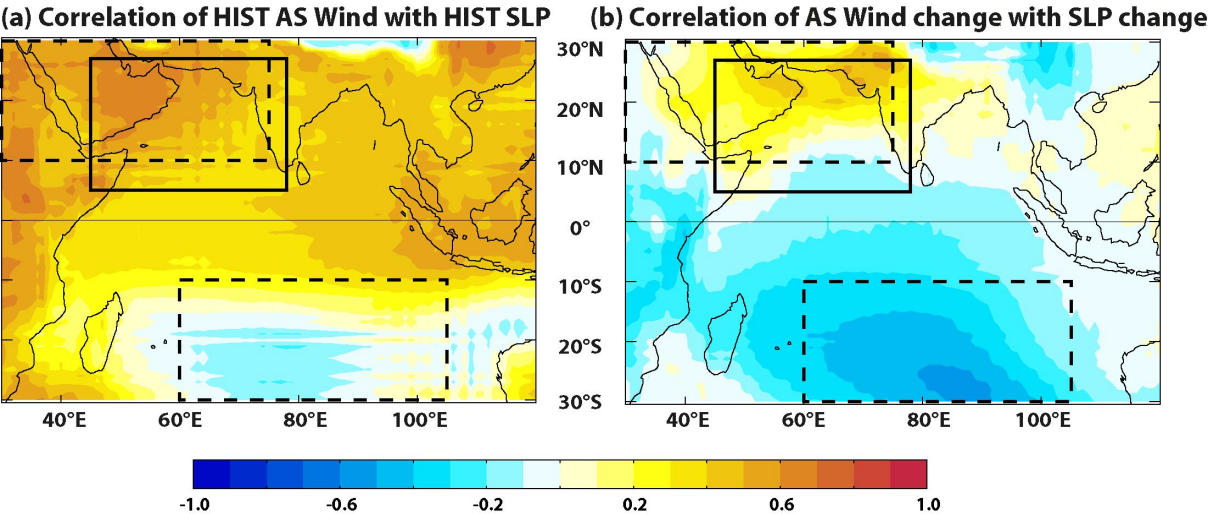


Figure S7. Map of correlation between (a) present-day average AS (black continuous frame) winter surface wind speed and winter SLP over IO and (b) same as (a), but for the projected changes.

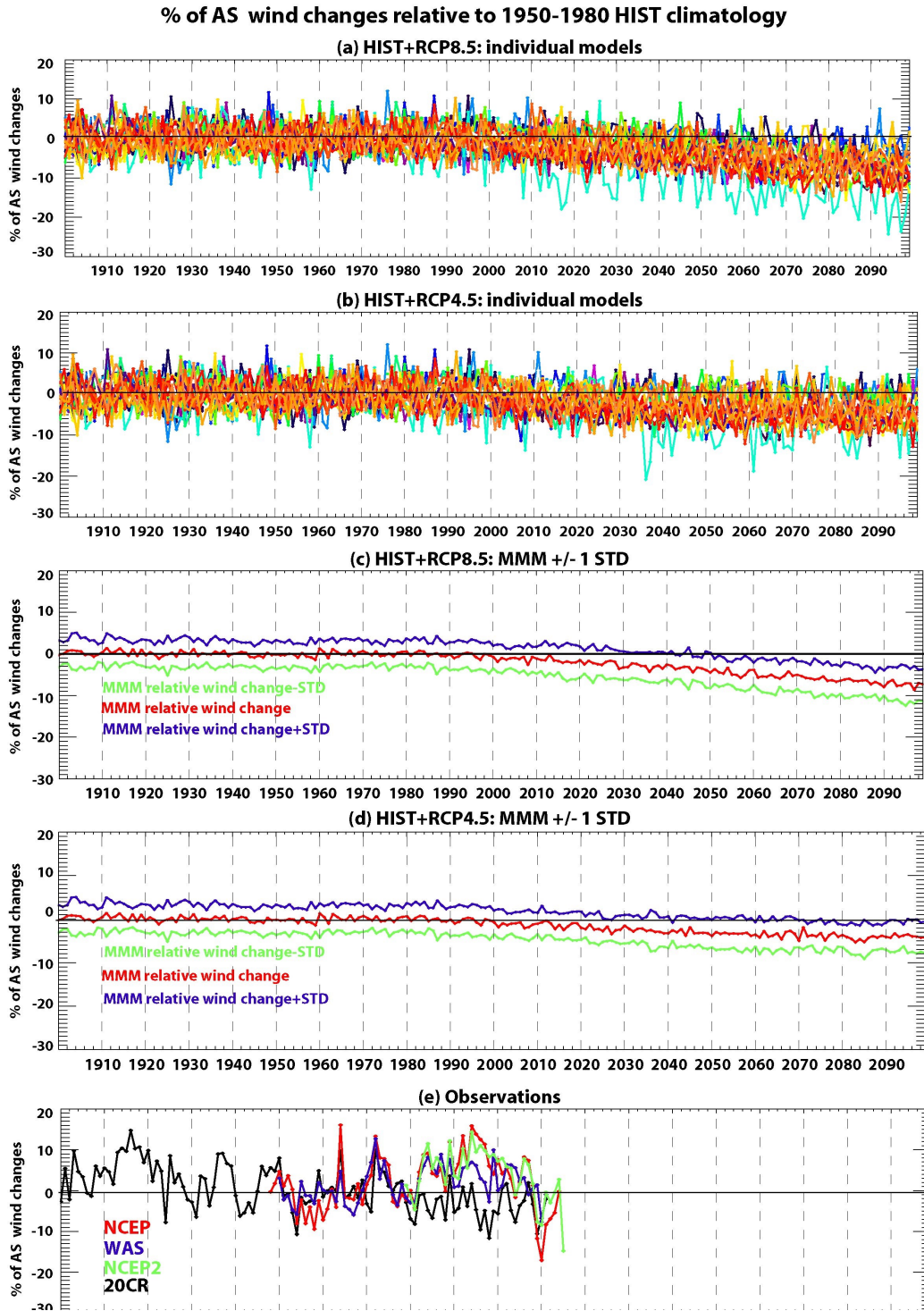


Figure S8. Percentage of average AS winter wind speed change relative to the 1950-1980 averaged climatology for (a) HIST and RCP8.5 simulations and (b) HIST and RCP4.5 simulations for each model. Percentage of CMIP5 MMM average AS winter wind speed change relative to the 1950-1980 climatology for (c) HIST and RCP8.5 simulations and (d) HIST and RCP4.5 simulations. The blue and green curves in panels c and d indicate +/- 1 standard deviation around the MMM. (e) Percentage of wind speed change in the AS relative to the 1950-1980 climatology from observationally-derived products: NCEP2 (green), NCEP (red), 20CR (black) and WASwind (blue).

Computational details for the corrected projections on the basis of current-day biases

In this paper, the projected response of some variables to climate change is corrected based on the present-day Arabian Sea wind bias. This correction method is basically the one followed by *Li et al.* [2016a]. The winter (DJFM) climatology for historical (last 20 years, i.e., 1986-2005) and the future (last 20 years; 2080-2099) scenarios are denoted respectively by $HIST(s,m)$ and $RCP(s,m)$, where ' s ' represents space (longitude-latitude) coordinates and ' m ' model IDs. The response to climate change for each model can then be calculated as the difference between the future and historical values.

$$Response(s,m) = RCP(s,m) - HIST(s,m) \quad (1)$$

The average AS winter surface winds bias is computed as the difference between the historical simulation average 1986-2005 surface winds minus that from observations as follows.

$$sfcwind'_{AS}(m) = sfcwindHIST_{AS}(m) - sfcwindO_{AS} \quad (2)$$

where $sfcwind'_{AS}$ is the average AS winter surface wind bias, $sfcwindHIST_{AS}$ is the average AS winter surface wind from historical simulations averaged and $sfcwindO_{AS}$ is the average AS winter Tropflux surface winds, all obtained for the 1986-2005 period.

The relationship between the projected AS surface wind changes and the present-day bias can be obtained through a linear regression analysis as,

$$Response(s,m) = a(s) * sfcwind'_{AS}(m) + b(s,m) \quad (3)$$

where $a(s)$ is the spatially-dependent regression coefficient and ' b ' is the residual. ' b ' can also be seen as the extrapolation of the projected response of climate change at zero bias, i.e. as the corrected response ($Response^*$) to climate change for each model.

$$Response^*(s,m) = b(s,m) \quad (5)$$

The MMM of the corrected response to climate change is calculated as:

$$(Response^*(s))_{MMM} = \frac{1}{N} \sum_{i=1}^N Response^*(s,m) \quad (6)$$

where N is the total number of models. The response of each model is expressed as the percentage of its current-day average winter surface wind over the AS. The figures provided in the text are the multi model mean of those percentages, with a 95% confidence limit computed using a Student t-test with $N-1$ degrees of freedom.